Scalar Transport and the Validity of Damköhler's Hypotheses for Flame Propagation in Intense Turbulence

Girish Nivarti* and Stewart Cant†

University Engineering Department,

Trumpington Street, Cambridge CB2 1PZ, UK

Abstract

The turbulent burning velocity of premixed flames is sensitive to the turbulence intensity of the unburned mixture. Premixed flame propagation models that incorporate these effects of turbulence rest on either of two hypotheses proposed by Damköhler. The first hypothesis applies to low-intensity turbulence which acts mainly to increase the turbulent burning velocity by increasing the flame surface area. The second hypothesis states that, at sufficiently high intensities of turbulence, the turbulent burning velocity is governed mainly by enhanced diffusivity. Most studies to date have examined the validity of the first hypothesis under increasingly high intensities of turbulence. In the present study, the validity of Damköhler's second hypothesis is investigated. A range of turbulence intensities is addressed by means of Direct Numerical Simulations spanning the "flamelet" and "broken reaction zones" regimes. The validity of Damköhler's second hypothesis is found to be strongly linked to the behaviour of turbulent transport within the flame.

* gvn22@cam.ac.uk

† rsc10@cam.ac.uk

I. BACKGROUND

A. Damköhler's first hypothesis and the flamelet regime

Prediction of turbulent burning velocity s_T is the central problem of practical interest in premixed turbulent flames. Formulations linking s_T to measurable effects of turbulence were pioneered by Damköhler [1]. The primary conclusion of Damköhler's study was that "turbulence always increases the flame speed referred to the average flow cross section, and in a two-fold manner" [2]. The first of these two "manners" concerns a regime where the turbulence length scales ℓ are large compared to the laminar flame thickness δ_L, i.e. $\ell \gg \delta_L$. Addressing this regime, Damköhler proposed [2] that

Hypothesis 1. *"for coarse-turbulence bodies exceeding the laminar flame thickness, the flame surface is effectively enlarged, which is, by roughening [the flame surface.] Thus the coarse-body turbulence effects a rise of the flame velocity, ..., even if the flame velocity in the individual surface elements is entirely the same as in laminar flow."*

wherein the flame velocity of individual surface elements refers to the local burning rate (or, equivalently, the flame speed). Damköhler argued further that the local velocity fluctuations u' which give rise to the "roughening" must balance the enhanced local burning rate s_T for the flame to be stable. This led to a linear relation $s_T \sim u'$. Hence, Damköhler's first hypothesis (hereby, DH1) may be summarised as

$$s_T = s_L \frac{A_T}{A_L} \implies s_T \sim u' \tag{1}$$

where A_T is the enlarged turbulent surface area and A_L is the appropriate flow cross-section area. The enhanced area ratio A_T/A_L, therefore, acts to magnify the locally laminar flame speed s_L to its equivalent s_T in turbulence. Interpreted as above, DH1 forms the basis of nearly all turbulent flame modelling to date.

Following the work of Damköhler, Karlovitz et al. [3] highlighted the influence of flow field effects that might arise in this regime, but might act instead to inhibit s_L. The resulting notion of flame stretch rate $\dot{s}$, defined as

$$\dot{s} = \frac{1}{A}\frac{dA}{dt}, \tag{2}$$

the fractional increase in flame surface area A over time, has helped describe a range of phenomena including extinction in Bunsen flames [4]. In laminar flames, the effects of flame stretch $\dot{s}$ on the flame speed s_L have been quantified comprehensively (as reviewed by Law [5]). In turbulent flames, it was proposed that [6, 7] flame stretch effects may be absorbed simply into DH1 using a factor $I_0 \lesssim 1$ under low levels of stretch, such that

$$\frac{s_T}{s_L} = I_0 \frac{A_T}{A_L}, \tag{3}$$

thereby modifying DH1 without invalidating its basic premise. Further, in order to address the difficulties in computing the exact area A_T of convoluted flame surfaces, a statistical approach was adopted. As an example, the Flame Surface Density (FSD, denoted by Σ) approach provides transport equations that can be written tractably for wrinkled flames [8, 9]. An equivalent description of DH1 has emerged [7] from this framework as follows

$$\frac{s_T}{s_L} = I_0 \frac{1}{A_L} \int_V \Sigma \, dv, \tag{4}$$

which is the same as Eq. 3 with A_T replaced by the integral of FSD over the flame brush volume V. Together with the stretch factor I_0, this description has helped account for inhibitive turbulent stretch effects on the local chemical structure. As a further consequence, the scope of DH1 has been extended to combustion regimes with small-scale turbulence wherein increasingly convoluted and stretched flames are observed.

A phenomenological description of turbulent stretch effects has emerged from the comparison of length scales involved in turbulent reacting flows. In this description, turbulent stretch is considered as the result of an interaction between the various length scales ℓ of turbulence and those of flame chemistry (such as δ_L). The local flame speed s_L (referred to in DH1) is expected to be "the same as in laminar flow" only if the Kolmogorov scale η (and all scales larger than it) is larger than δ_L. The size of these turbulent microscales is inversely related to the intensity u' of a homogeneous isotropic turbulent flow field according to $\eta \propto (\nu/u')^{1/2}$ for a given integral scale ℓ_0 [10]. Hence, DH1 is expected to be strictly valid for a turbulent flow with a specified ℓ_0 if u' is low enough that $\eta > \delta_L$.

The Karlovitz number $\mathrm{Ka} \equiv \delta_L^2/\eta^2$ is a dimensionless marker that delineates the regimes of turbulence-flame interaction by quantifying the comparison of length scales. Ka may be

estimated using the formulation for stretch experienced by a scalar surface due to turbulence at the Taylor microscale [11]

$$\mathrm{Ka} = \mathrm{Re}_0^{-\frac{1}{2}} \left(\frac{u'}{s_L} \right)^2, \tag{5}$$

expressed in terms of chemical parameters: s_L and δ_L, and physical parameters: turbulence intensity u' and integral length scale ℓ_0 (by the turbulent Reynolds number $\mathrm{Re}_0 = u'\ell_0/\nu$). In Fig. 1, isolines of Ka and Re have been used to show the regimes of turbulence-flame interaction in the Borghi diagram. Damköhler's regimes, DH1 (as described above) as well as DH2 (to be discussed below) correspond to regions in the deigram with contrasting values of length scales ($\ell_0 \gg \delta_L$ and $\ell_0 \ll \delta_L$) along a constant Re isoline (as discussed in §5 of [2]). The "flamelet" regime satisfies the Klimov-Williams criterion $\mathrm{Ka} < 1$ and, hence, DH1 is expected to be valid in this regime based on the phenomenological description.

B. Intense Turbulence and Damköhler's second hypothesis

Many experiments (reviewed in [12, 13]) have reported a departure from the linear relation $s_T \sim u'$ (which is implied by DH1) in turbulent premixed flames with $\mathrm{Ka} > 1$. This so-called "bending effect" of the $s_T(u')$ curve has been isolated to occur when all parameters but u' are maintained constant [12–14] (within the parameter space consisting of u', ℓ_0, s_L, and δ_L). It has been suggested that bending marks the onset of a departure from the locally

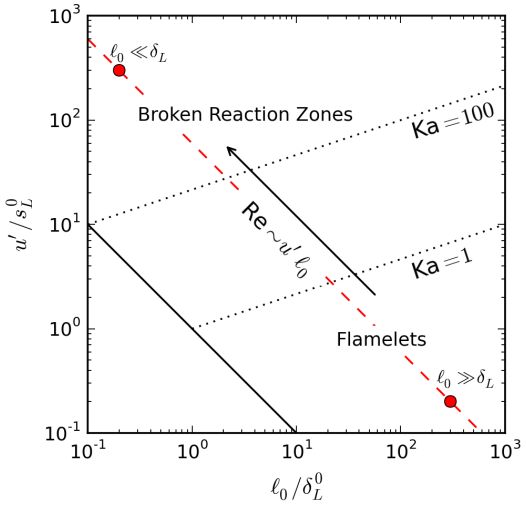

FIG. 1: Regimes proposed by Damköhler [1] illustrated on the Borghi diagram. DH1 and DH2 correspond to the limiting regimes $\ell_0 \gg \delta_L$ and $\ell_0 \ll \delta_L$ respectively.

flamelet structure – the foundational basis of DH1 – leading to quenching of the flamelet [15]. A Direct Numerical Simulation (DNS) study of 2D single-eddy-flame interactions [16] has shown, however, that the area enhancement mechanism of DH1 may remain valid despite local flamelet quenching. Consequently, models have been developed [17] on the assumption that DH1 persists (up to Ka $\approx$ 16) so long as quenching "does not inhibit the growth of the active flame surface" [18]. Experimental studies have since correlated s_T data within the extended DH1 framework (Eq. 3 and Eq. 4), reformulating the stretch factor I_0 as a "burning factor" $P_b \sim I_0^2$ instead [11].

In contrast, many computational investigations have corroborated the resilience of the flamelet structure (especially, the reaction zone) to intense turbulence [13, 19–22]. As a result, a description of bending in the absence of flamelet quenching is sought [23]. Fig. 2 shows the $s_T(u')$ curve computed in a recent DNS study [24] which presented the bending effect recorded for $u' > 10$ as the result of an underlying competition between stretch-rate components (strain and curvature terms). Hence, an explanation of the bending effect was proposed which does not invoke flamelet quenching. More recent DNS simulations and their comparison with experiments at high u' [25] support the plausibility of such an explanation. Some experiments, however, have provided contrary evidence and disputed the persistence of flamelet structure as well as the validity of DH1 in moderate to intense turbulence [26, 27]. Subsequent DNS studies have, therefore, focused on illuminating further the role of quenching at high u' [28–30].

Nearly all of these investigations have focused on the validity of DH1 at increasingly high values of u'. A second hypothesis proposed by Damköhler [1] (here called DH2) concerns the limiting regime of high u' turbulence wherein $\ell_0 \ll \delta_L$ (as shown in Fig. 1). Addressing this regime, contrasting with DH1, Damköhler proposed [2] that

Hypothesis 2. *for fine-body turbulence, . . . , an amplification of every microscopic transport process in the flame surface must occur, especially between the reaction zone and the pre-heat zone. These transport processes [then] . . . govern the flame speed decisively.*

wherein the microscopic transport processes referred to may be molecular diffusion or thermal conduction. In laminar flames, the molecular diffusion coefficient $\mathcal{D}_L$ and the reaction rate $\dot{\omega}$ together govern the flame speed according to $s_L \sim \sqrt{\mathcal{D}_L \dot{\omega}}$ [31, 32] for unity Lewis number Le = 1. The mass fraction Y_α of a suitable chemical species (or temperature T) may

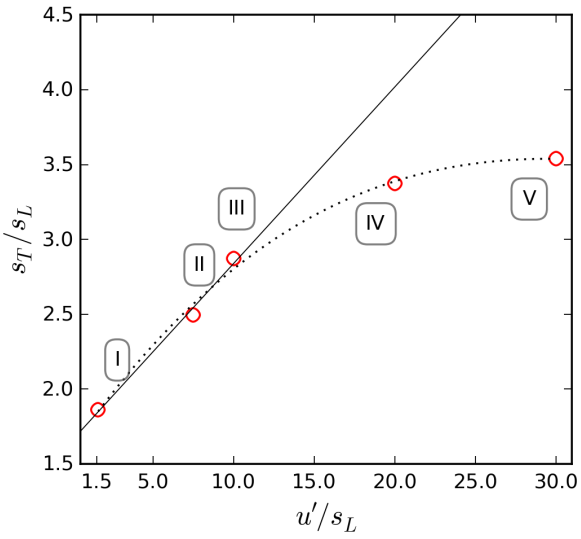

FIG. 2: The bending effect in $s_T(u')$ captured by recent DNS [24]. At high u', there are diminishing increments in s_T with increasing u'.

then be used to quantify the extent of chemical reaction using a progress variable defined as $c = (Y_\alpha^u - Y_\alpha)/(Y_\alpha^u - Y_\alpha^b)$ (the subscripts u and b denote unburned and burned components respectively) such that $c = 0$ in unburned reactants and $c = 1$ in burned products. For statistically-1D turbulent flames, the Favre mean progress variable $\tilde{c}$ provides an equivalent framework [33]. In this framework, the convective-diffusive-reactive balance that governs turbulent premixed flame propagation may be written as

$$\nabla \cdot \bar{\rho}\tilde{\mathbf{u}}\tilde{c} = -\nabla \cdot \bar{\rho}\widetilde{\mathbf{u}''c''} + \overline{\dot{\omega}}, \tag{6}$$

provided $\mathrm{Re} \gg \mathrm{Da} \gg 1$ so that the molecular transport term can be neglected. Favre mean quantities $\widetilde{q} = \overline{\rho q}/\bar{\rho}$ represent density-weighted averages whereas q'' denotes the respective fluctuations, i.e. $q = \tilde{q} + q''$. This framework forms the basis for several modelling approaches for turbulent combustion including the Bray Moss Libby (BML) formulation [34]. Here, the propagation of the mean flame surface $\tilde{c}$ (l.h.s. in Eq. 6) is linked with two aspects (terms on the r.h.s. in Eq. 6): 1) the scalar flux term $-\nabla \cdot \bar{\rho}\widetilde{\mathbf{u}''c''}$ which describes turbulent mixing across the $\tilde{c}$ iso-surface and 2) the reaction source-term $\overline{\dot{\omega}}$ which describes the transformation of $\tilde{c}$ from $0 \longrightarrow 1$. The first term operates favourably towards flame propagation when the

turbulent scalar flux $\widetilde{u''c''}$ (in the x-direction, say) follows

$$\widetilde{u''c''} = -\mathcal{D}_T \frac{\partial \widetilde{c}}{\partial x}, \tag{7}$$

a gradient transport expression analogous to the diffusive mixing of a passive scalar [35]. This expression models the transport of the scalar flux $\widetilde{u''c''}$ down the mean scalar gradient $\partial\widetilde{c}/\partial x$ for a positive diffusion coefficient $\mathcal{D}_T > 0$. As a result, the ratio $\mathcal{D}_T/\mathcal{D}_L$ denotes the enhancement of diffusive transport processes (referred to in DH2) predominantly due to turbulence small-scales.

Reasoning along these lines, Damköhler described the enhancement of s_T in "fine-body" turbulence using the formulation

$$\frac{s_T}{s_L} = \sqrt{\frac{\mathcal{D}_T}{\mathcal{D}_L}}, \tag{8}$$

borrowing the square root by analogy to the dependence $s_L = f(\sqrt{\mathcal{D}_L})$ observed in laminar flames. It follows that the ratio $\mathcal{D}_T/\mathcal{D}_L$ (and, hence, $\mathcal{D}_T$ itself) must remain positive in order to preserve the mathematical validity of DH2.

Numerical [36, 37] and experimental studies [38] have illustrated, however, that this is not necessarily the case. In other words, the turbulent scalar flux $\widetilde{u''c''}$ (l.h.s. in Eq. 7) does not always have the opposite sign (direction) to the scalar gradient $\partial\widetilde{c}/\partial x$ (r.h.s. in Eq. 7). In such a case, Eq. 7 provides $\mathcal{D}_T < 0$ posing a threat to the validity of the DH2 expression (Eq. 8). Under such conditions, turbulent scalar transport is said to occur in a counter-gradient (CG) fashion [36].

CG transport has been attributed [39] to the shift in balance between flame-induced gas expansion (represented by τ) and flow-imposed turbulent fluctuations (represented by u'). An appropriate model that captures the accompanying change in sign of $\widetilde{u''c''}$ is written [39] as follows

$$\widetilde{u''c''} = \tilde{c}(1-\tilde{c})\left(\tau s_L - 2\alpha u'\right), \tag{9}$$

wherein the ratio $N_B = \tau s_L/2\alpha u'$ (called the Bray number) dictates the CG/G transition in scalar flux transport (since $\tilde{c}(1-\tilde{c}) > 0\ \forall \tilde{c} \in [0,1]$). DNS analysis of mean scalar flux transport has highlighted the role of fluctuating and mean pressure gradients [37, 39] in the CG/G transition. The influence of flame-generated vorticity has also been investigated [40]. Wenzel and Peters [19] have verified the role of gas expansion in their simulations of the

flame surface using the G-equation with added heat release. These simulations recorded a bending effect in $s_T(u')$ accompanying the CG/G transition as is the case in the recent dataset produced by the present authors [24]. Despite these insights, the implication of scalar transport mechanisms on the formulations for s_T enhancement remains to be addressed. In particular, a connection of the CG/G transition with the DH2 expression for s_T has not been considered to date.

Damköhler proposed each of the two hypotheses to elucidate the primary mechanism of s_T enhancement in their respective regimes of turbulence. While this primary mechanism operates, the secondary mechanism was expected to "recede in the background" contributing alongside albeit to a lesser degree. Over the years, the range and upper u' limit of validity for DH1 has received significant attention. However, the lower u' limit of validity for DH2 remains unknown. Recent investigations in intense [21, 29] and extreme [41] u' turbulence have highlighted the significance of diffusive transport processes in determining s_T under such conditions. Appropriate modifications of DH2 are being proposed so as to fit the s_T data acquired. Motivated by these investigations, the present work focuses on outlining the regimes where DH2 is applicable. A CG/G transition recorded using DNS is analysed and its implication on the minimal condition of validity for DH2 is discussed.

II. PROBLEM SETUP

A statistically-planar turbulent configuration is simulated within a 3D cuboidal inflow-outflow domain. A turbulent flow-field of required intensity is initialized within the domain and is also convected at a mean speed $\langle u_i \rangle = s_L$ through the inlet. Fig. 3 illustrates this configuration by showing a typical snapshot obtained from one of the simulations. The flame, represented here by a single isosurface (red), propagates into upstream turbulence (grey eddies) with a speed s_T (red arrow). The domain is 3 times as long as it is wide ($L_x = 3L_y = 3L_z$ as reported in Tab. I) so as to accommodate flame propagation and in order to avoid flame-boundary interactions. Inlet and outlet faces have been marked with blue arrows in Fig. 3, whereas the remaining faces are periodic. Details of the simulation methodology are presented in the following passages.

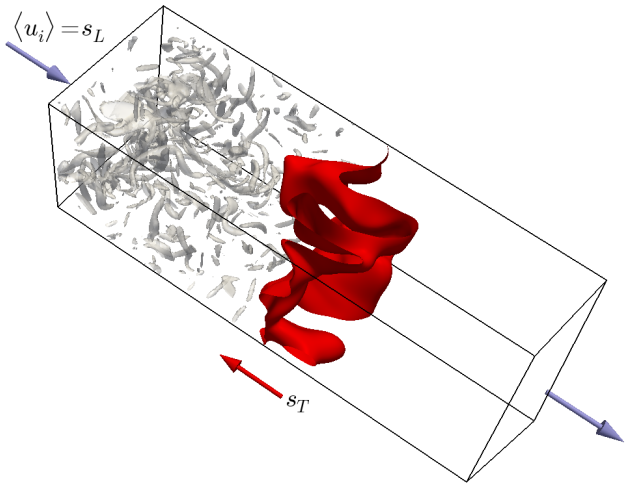

FIG. 3: The inflow-outflow configuration where a statistically-planar flame propagates into the surrounding turbulent flow field.

A. Turbulence Initialisation and Inflow

Initial turbulence is computed using a procedure outlined by Rogallo [42] as follows. A homogeneous isotropic turbulent velocity field of desired turbulence intensity u' is generated using the Batchelor-Townsend (BT) spectrum [43]. The BT spectrum is specified in Fourier space using two parameters: 1) u', which corresponds to the turbulent kinetic energy and 2) k_0, the wavenumber of peak turbulent kinetic energy. The corresponding Cartesian field is then computed by Fourier transform and initialised in a cubic periodic domain. This Cartesian periodic velocity field is allowed to evolve briefly and is stored for turbulence initialisation and inflow in the flame simulations.

Each individual flame simulation case (with specified u') is simulated in a domain 3 times the length of the cubic domain. The velocity field in this domain is initialised by placing adjacently 3 copies of the turbulent flow field generated *a priori* (according to the description above). Yet another copy is convected through the inlet as inflow so as to maintain u' within the domain. A statistically-stationary spatial profile with a power-law decay of turbulence is established upstream of the flame within a few eddy turn-over times. Hence, the turbulence imposed upon the flame corresponds to a range of intensities from as high as the inlet/initial turbulence intensity u'_i (calculated at the inlet or at $t = t_0$) down to as low as the flame leading-edge turbulence intensity u'_{le} (calculated at the $\langle c \rangle = 0.001$ section of the domain). These quantities are reported in Tab. I.

The regime diagram is shown in Fig. 4 where the Karlovitz number has been calculated

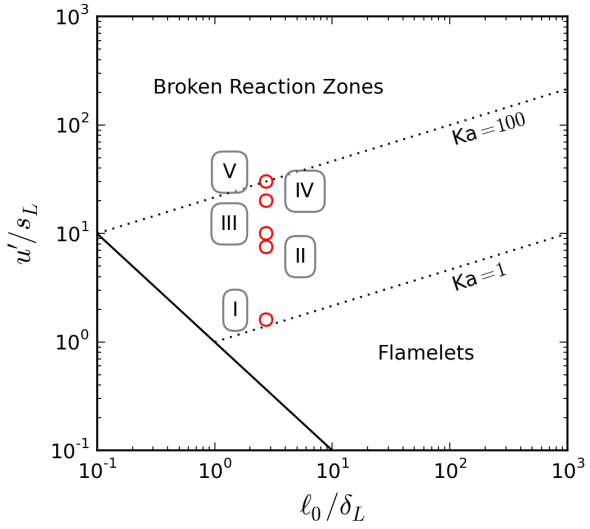

FIG. 4: The regimes spanned by the dataset estimated based on the initialised turbulence and thermo-chemical parameters.

based on Eq. 5 using inlet/initial turbulence parameters. By increasing u' successively between each simulated case, the dataset bridges the flamelet regime and the broken reaction zones regime. The parameters k_0 and the domain width ($L_y = L_z$, reported in Tab. I) specify together the integral length scale ℓ_0 and are fixed throughout the dataset. Hence, u' is the only parameter varied across the dataset with the physical consequence that the turbulence small-scales $\ell < \delta_L$ become progressively smaller from case I to case V.

In order to capture large-scale wrinkling, the integral length scale is chosen to be larger than the laminar flame thickness: $\ell_0 \sim 3\delta_L$. The Batchelor-Townsend spectrum [43] used to initialise turbulence as above provides an expression for the Kolmogorov scale η as

$$\eta = \left[\frac{\nu^2}{15\pi^2 u'^2 k_0^2}\right]^{1/4} \tag{10}$$

where ν is the kinematic viscosity and u' and k_0 are pre-specfied parameters as described above. Since the integral scale ℓ_0 is fixed across all simulations, the Kolmogorov scale η becomes very small in high u' turbulence. Hence, complete resolution of high u' turbulence up to the Nyquist frequency imposes a severe computational challenge. Hence, the fixed mesh spacing is chosen as $\Delta x \sim \mathcal{O}(\eta)$ in order to resolve the smallest scales for all cases. Nevertheless, the adequacy of resolution is assessed using the criterion proposed by Poinsot et al. [44] written as $\mathrm{Re_0Da} < 2(1+\tau)^{0.7}(N_y/m \times n_e)^2$ [45, 46]. Given that up to $n_e \approx 5$

TABLE I: Upstream turbulence properties and dimensionless parameters for each of the 5 simulated cases.

Case $\longrightarrow$			I	II	III	IV	V
Inlet/Initial u'	u'_i/s_L		1.50	7.50	10.00	20.00	30.00
Leading-edge u'	u'_{le}/s_L		0.94	4.50	6.00	12.00	18.00
Turbulent KE	k	m^2/s^2	0.6	11.7	20.6	82.5	185.6
Peak KE wavenumber	κ_0				2.0		
Integral length scale	ℓ_0	mm	$\longleftarrow$		0.99		$\longrightarrow$
Kolmogorov scale	η	μm	74.59	33.35	28.89	20.42	16.67
Domain length	$L_x = 3$	cm			1.5		
Domain width	L_y, L_z	cm	$\longleftarrow$		0.5		$\longrightarrow$
Grid size	$N_x \times N_y \times N_z$		$\longleftarrow$		$288 \times 96 \times 96$		$\longrightarrow$
Axial mesh resolution	Δx	μm			52.26		
Span-wise resolution	$\Delta y, \Delta_z$	μm			52.63		
LETOT	τ_0	ms	1.59	0.34	0.25	0.12	0.08
Chemical time	τ_c	ms	0.93	0.93	0.93	0.93	0.93
Total run time	$T = 4\tau_0$	ms	6.36	1.28	1.0	0.48	0.32
Reynolds number	Re_0		39.28	184.13	245.51	491.03	736.51
Damköhler number	Da		1.71	0.36	0.27	0.13	0.09
Karlovitz number	Ka		1.20	12.36	19.08	53.96	99.82

† Arrows indicate that empty fields have the same value as the centre column field of the corresponding row.
* Acronyms: LETOT (Large-Eddy Turn-Over Time) and KE (Kinetic Energy).

integral length scales are accommodated in the domain width consisting of N_y points, and the flame is resolved by up to $m \approx 8$ points (discussed below), the criterion is found to be satisfied for the entire dataset. This level of resolution is considered adequate here, especially for addressing the central goal which is to connect conceptually the validity of Damköhler's second hypothesis with a possible onset of counter-gradient transport. Subsequent refinement of the mesh size to satisfy $\Delta x < \eta/2$ in the highest-intensity cases is expected to substantiate this investigation further and is, therefore, being pursued as part of ongoing work. Physical parameters, length scales, and dimensionless groups relevant to the dataset have been listed in Tab. I.

1. *Calculation of laminar flame speed and thickness*

Evidently, the choice of u' and ℓ_0 necessary for specifying the combustion regime is guided by the knowledge of laminar flame speed s_L and thickness δ_L. These properties are evaluated from the numerical solution of an unstrained 1D laminar premixed flame (i.e. $s_L = s_L^0$ and $\delta_L = \delta_L^0$) computed *a priori* (using the chemical mechanism described below).

TABLE II: Thermo-chemical input parameters.

Ambient pressure, P_0	1.01×10^5 Pa
Inlet temperature, $T_in = T^u = T_0$	300 K
Adiabatic flame temperature, $T_{ad} = T^b$	2300 K
Pre-exponential constant, B	2.75×10^7 $\mathrm{m^3kg^{-1}s^{-1}}$
Activation energy, E_a	10^8 $\mathrm{Jkg^{-1}}$
Gas constant, R	$287.1\mathrm{Jkg^{-1}K^{-1}}$
Molecular transport constant, A_λ	2.585×10^{-5}
Molecular transport exponent, r	0.7
Lewis number, Le	1.0
Prandtl Number, Pr	0.7
Schmidt Number, Sc	0.7
Equivalence ratio, ϕ	1.0
Gas expansion factor, τ	6.67
Laminar flame speed, $s_L = s_L^0$	0.39 $\mathrm{ms^{-1}}$
Laminar flame thickness, $\delta_L = \delta_L^0$	3.6×10^{-4} m

The laminar flame speed s_L is obtained by integrating the reaction rate $\dot{\omega}_R$ across the domain. This calculation may be generalised as a volume-integration to obtain the flame speed s_T of a 3D turbulent premixed flame. Hence,

$$s_{L,T} = -\frac{1}{\rho_R^u Y_R^u} \int_V \dot{\omega}_R(\vec{x})\, dv, \tag{11}$$

where Y_R^u is the upstream/unburned reactant mass fraction and ρ_R^u is the corresponding density, while $\dot{\omega}_R(\vec{x})$ is the reaction rate of reactants at any point $\vec{x}$ in the domain.

The laminar flame thickness δ_L is obtained using the maximum-temperature-gradient method

$$\delta_L = \frac{T^b - T^u}{(dT/dx)_{max}} \tag{12}$$

where T^u and T^b are the unburned and burned gas temperatures respectively. Approximately 8 points resolve the laminar flame thickness in the present simulations; the sufficiency of this resolution level was established using a mesh convergence study which showed that the internal structure can be simulated accurately with as few as $5-6$ points across the flame thickness. The values of s_L and δ_L are provided in Tab. II. Details of the chemical mechanism and thermo-chemical initialisation are provided below.

B. Thermochemical Initialisation and Chemistry

The initial thermo-chemical field for the flame simulation (density ρ, temperature T, and species mass-fractions Y_α) is specified using an unstrained 1D laminar flame solution profile calculated *a priori* with the desired stoichiometry $\phi = 1.0$ and inlet conditions. The premixed methane-air laminar flame chemistry is described using a single-step Arrhenius expression as follows

$$\dot{\omega}_\alpha = B\rho Y_\alpha T^n e^{-E_a/(RT)}, \tag{13}$$

where the constants B, E_a, and R are listed in Tab. II. In order to calculate the diffusive mass flux for each species α, a Fickian law is used as follows

$$\rho V_{\alpha,k} Y_\alpha = -\rho \mathcal{D}_\alpha \frac{\partial Y_\alpha}{\partial x_k} \tag{14}$$

where $V_{\alpha,k}$ is the diffusion velocity of species α in the k direction. The molecular transport coefficients are calculated based on the relationship [47]

$$\frac{\lambda}{C_p} = A_\lambda \left(\frac{T}{T_0}\right)^r \tag{15}$$

for the mixture thermal conductivity λ, where C_p is the mixture value of the specific heat capacity at constant pressure and A_λ, r, and T_0 are constants (listed in Tab. II). The mixture dynamic viscosity μ is calculated from the transport coefficients as $\mu = \lambda C_p/\mathrm{Pr}$ based on a constant Prandtl number $\mathrm{Pr} = 0.7$. The relevant thermo-chemical input parameters along with ambient conditions have been tabulated in Tab. II.

The thermochemical framework of single-step chemistry with unity Lewis number provides a basic set of conditions to investigate the salient mechanisms of a combustion phenomenon. The applicability of this framework may be restricted with regard to the accurate description of the reaction zone. For example, in lean premixed hydrogen-air flames, small turbulent scales may cause chemical source term fluctuations at high Karlovitz numbers when simulated using detailed kinetics [28, 48]. Additionally, differential diffusion effects may still be important at such high Karlovitz numbers [30, 48]. However, the focus here is on studying the effects of turbulence small-scales on the transport processes. The CG/G transition captured in the present work (as discussed below), therefore, is expected to shed

light on the possible limitations of DH2 and is not restricted significantly by the thermo-chemical framework adopted.

III. NUMERICAL METHOD

The Navier-Stokes equations are solved in a 3D compressible form along with thermo-chemical transport using the `SENGA2` DNS code [49]. A 10^{th}-order centred finite difference operator evaluates spatial derivatives and reduces to 4^{th} order at inlet and outlet faces (details of the difference scheme is discussed in the User Manual [49]). In the stream-wise direction, inflow-outflow boundaries are specified using the Navier-Stokes characteristic boundary conditions [50]. At the inlet, a reflecting constant density condition with specified velocity components is imposed, whereas at the outlet, a non-reflecting outflow condition is imposed. The transverse direction faces are specified with periodic boundary conditions. A 4^{th}-order explicit Runge-Kutta method is used for time-marching along with adaptive time-stepping implemented using an error controller [51]. The `DARWIN` (Intel Sandy Bridge E5-2670) and `ARCHER` (Cray XC30) supercomputers were used to compute the solutions. Each simulation used approximately $\sim 2.5 \times 10^4$ core-hours.

IV. BACKGROUND TO THE ANALYSIS

In the simulations conducted as described above, the principal quantity of interest, the turbulent flame speed s_T, evolved to a value specific to each case after a brief initial period of development $0 < t < 2\tau_0$. Subsequent to this period, s_T fluctuated about this value for the remaining duration of up to $t \sim 4\tau_0$. The existence of a reasonably well-defined mean value was considered as an indication of statistically-stationary (as discussed in [24]). The data analysed below has been collected at $t = 4\tau_0$ corresponding to each of the cases. Averaging, where implied, is conducted over spanwise directions as before [24].

A. Molecular diffusivity

The molecular diffusivity $\mathcal{D}_L$ of a species in laminar flow is calculated as

$$\mathcal{D}_L = \frac{\lambda}{\rho C_p \mathrm{Le}}, \tag{16}$$

given its Lewis number (here, Le = 1.0). As quoted in Sec. I B, DH2 refers to the turbulent amplification of molecular diffusion "between the preheat zone and the reaction zone". In order to produce the diffusion coefficients for evaluating DH2, values must then be chosen within this ($0.6 \leq c \leq 0.9$) region. In the present work, $\mathcal{D}_L$ is calculated as $\mathcal{D}_L = (\lambda/\rho C_p)|_{c=0.8}$ at $c = 0.8$ where the reaction rate attains a maximum in a laminar flame. Similarly, the turbulent diffusivity $\mathcal{D}_T$ is evaluated at $\tilde{c} \approx 0.8$ in the turbulent premixed flame brush. In Damköhler's original work [1, 2], $\mathcal{D}_T$ was estimated using Prandtl's hypothesis [52]. More recently [13, 29], $\mathcal{D}_T$ has been calculated using parameters of the $k-\epsilon$ model of turbulence. Since the present study is focused on investigating the ramifications of using the gradient hypothesis, $\mathcal{D}_T$ is calculated based on Eq. 7 as

$$\mathcal{D}_T = -\frac{\widetilde{u''c''}}{\partial \tilde{c}/\partial x}\bigg|_{\tilde{c}=0.8}. \tag{17}$$

B. Damköhler's First Hypothesis

The dataset [24] obtained by the method described above recorded a bending effect in the $s_T(u')$ curve (as shown previously in Fig. 2). The area ratio A_T/A_L corresponding to instantaneous reaction surface ($c = 0.8$) was calculated for each case. Fig. 5 shows that this ratio A_T/A_L tracks s_T/s_L with significant accuracy (barring a slight deviation noted for the highest intensity case V). In other words, DH1 retains its validity throughout the recorded $s_T(u')$ curve. Similarly strong correlations between A_T/A_L and s_T/s_L have been reported by Lapointe and Blanquart [53] based on DNS of high Karlovitz number flames using detailed chemistry. This implies that the "roughening" action of turbulence large-scales $\ell \gg \delta_L$ describes accurately the enhancement of s_T. What then is the role of turbulence small-scales $\ell < \delta_L$? In the following passages, the role of small-scales in the amplification of diffusive processes (as suggested in DH2) is assessed within the same dataset.

V. RESULTS

In Fig. 6, each panel shows the variation of Favre averaged turbulent scalar flux $\widetilde{u''c''}$ with the Favre averaged scalar gradient $\partial\tilde{c}/\partial x$ for the specified case with corresponding u'. Each point in a panel ($\partial\tilde{c}/\partial x$, $\widetilde{u''c''}$) is coloured according to the corresponding value of $\tilde{c}$, indicating its position in the mean flame brush $0.01 < \tilde{c} < 0.99$. The leading edge $\tilde{c} \approx 0$ (cold unburned reactants) is coloured blue, whereas the trailing edge $\tilde{c} \approx 1$ (hot burned products) is coloured red. In all of the cases, $\partial\tilde{c}/\partial x > 0$ throughout the mean turbulent flame brush, i.e. points lie to the right of the dotted vertical line at $\partial\widetilde{c}/\partial x = 0$. An exception is the small region close to $\tilde{c} \approx 0.6$ (marked light-red points in Fig. 6c) in case IV which is attributed to excessive entrainment of unburned reactants within the preheat zone of the mean flame brush (seen later in Fig. 7). In contrast, the scalar flux $\widetilde{u''c''}$ transitions from being entirely positive to entirely negative across the different cases. Four representative cases (I, III, IV and V) are discussed below to highlight the salient features of this transition.

In case I (Fig. 6a), $\widetilde{u''c''} > 0$ throughout the Favre mean flame brush. In addition, $\widetilde{u''c''}$ appears to have a direct correspondence with mean scalar gradient $\partial\tilde{c}/\partial x$, both terms attaining a maximum in the preheat zone between $\widetilde{c} \approx 0.4$ and $\widetilde{c} \approx 0.6$. Similarly, case II (not shown) as well as case III (Fig. 6b) exhibit $\widetilde{u''c''} > 0$ across most of the brush; i.e. all

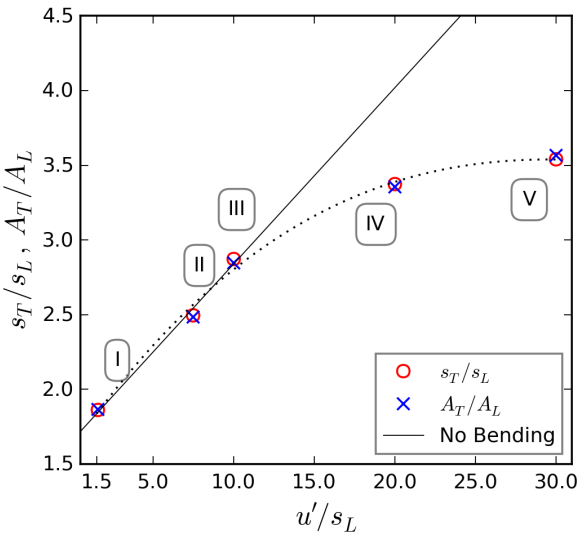

FIG. 5: Computed normalized turbulent burning velocity s_T/s_L provides an excellent match when compared with the area ratio A_T/A_L. Only close inspection reveals minor differences between the two ratios in high u' turbulence.

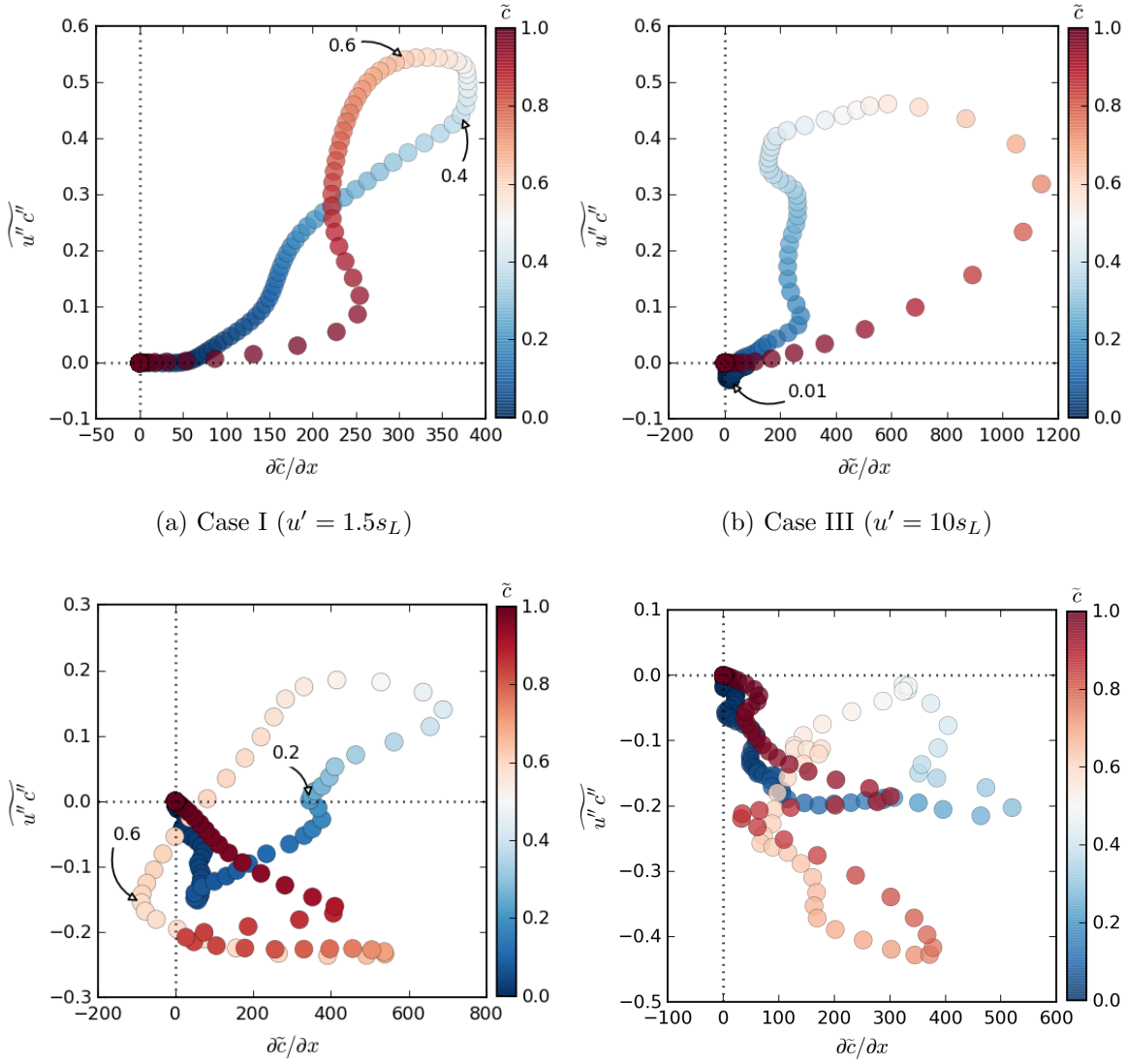

(a) Case I ($u' = 1.5s_L$)

(b) Case III ($u' = 10s_L$)

(c) Case IV ($u' = 20s_L$)

(d) Case V ($u' = 30s_L$)

FIG. 6: Variation of mean scalar flux $\widetilde{u''c''}$ with the mean scalar gradient $\partial\tilde{c}/\partial x$. Colours represent corresponding values of the mean progress variable $\tilde{c}$ within the turbulent flame brush (blue: leading edge $\tilde{c} = 0.01$, red: trailing edge $\tilde{c} = 0.01$).

points lie above the dotted horizontal line. The correspondence of $\widetilde{u''c''}$ with $\partial\tilde{c}/\partial x$ follows in similar fashion, but with the exception that $\widetilde{u''c''} < 0$ close to the leading edge, exhibiting a local minimum close to $\widetilde{c} \approx 0.01$ (marked dark blue dots in Fig. 6b). Clearly, the upstream turbulence intensity u' in case IV begins to overturn the counter-gradient (CG) transport $\widetilde{u''c''} > 0$ that existed throughout the flame brush in the low u' case I. This shift in the behaviour of $\widetilde{u''c''}$ in the preheat zone is, therefore, a signature of the imminent transition to gradient (G) transport at higher intensities.

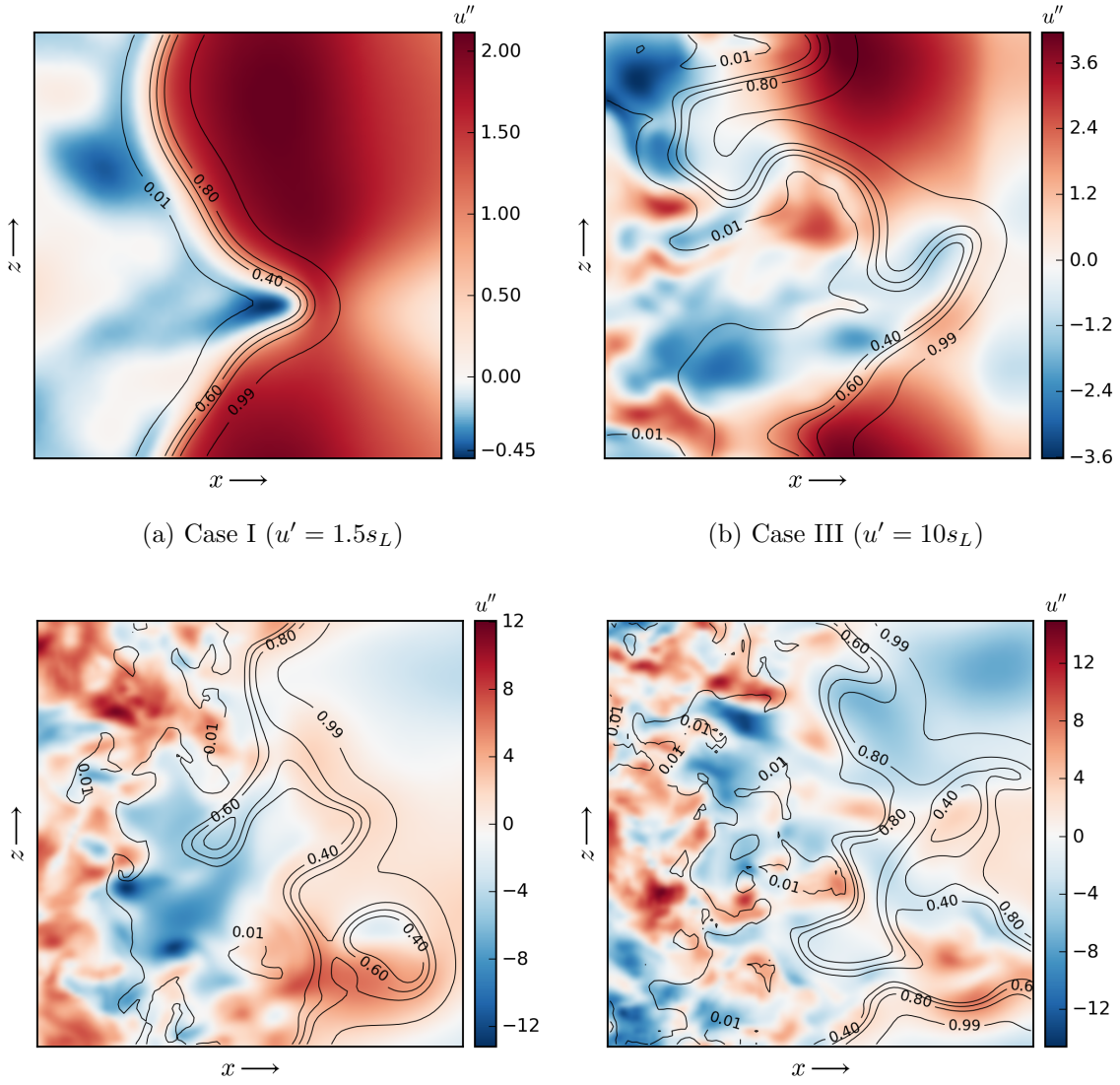

(a) Case I ($u' = 1.5s_L$)

(b) Case III ($u' = 10s_L$)

(c) Case IV ($u' = 20s_L$)

(d) Case V ($u' = 30s_L$)

FIG. 7: Instantaneous flame surface contours (black lines) and Favre velocity fluctuations u'' (background colours) in a cross-section ($y = \frac{L_y}{2}; \frac{L_x}{3} < x < \frac{2L_x}{3}, z$) of the domain.

Upon increasing u', the magnitudes of $\widetilde{u''c''}$ and $\partial\tilde{c}/\partial x$ do not change significantly (as seen in the axes of panels in Fig. 6). Instead, the sign of $\widetilde{u''c''}$ and the correspondence between $\widetilde{u''c''}$ and $\partial\tilde{c}/\partial x$ is affected considerably. In case IV (Fig. 6c), $\widetilde{u''c''} < 0$ through most of the flame brush (barring a small region between $\tilde{c} \approx 0.2$ and $\tilde{c} \approx 0.6$) whereas in case V (Fig. 6d), $\widetilde{u''c''} < 0$ across the entire flame brush. The high degree of scatter that accompanies this transition marks a departure from a smooth wrinkled flame to a highly convoluted flame.

Fig. 7 shows flame surface contours corresponding to the cases I, III, IV and V within streamwise slices of the domain (the flame is propagating to the left). The departure from a smooth wrinkled flame in case I to the highly convoluted flame in cases IV and V is seen readily. This corresponds to the contrast in scatter of points in the respective cases noticeable in Fig. 6. Such a change in the pattern of wrinkling was also reflected in the CG/G transition captured in other simulations conducted previously [39, 54].

Each panel of Fig. 7 also shows the velocity fluctuations u'' using colours (blue: negative, and red: positive) in the backdrop of the contour lines. The decreasing size of turbulence small-scales with increasing u' may be observed in the gradually changing distribution of coherently coloured flow field regions. On closer inspection, it is seen additionally that while positive velocity fluctuations (red colour) appear predominantly behind the flame in case I (Fig. 7a), such fluctuations appear ahead of the flame to a significantly higher extent in case V (Fig. 7d). This transition provides visual evidence of a shift in balance within the dataset between velocity gradients of two varieties: 1) those *generated* behind the flame due to gas expansion, and 2) those *present* ahead of the flame in the turbulent flow field.

The role of the balance between the flame imposed gas expansion and the flow imposed turbulence in the CG/G transition was investigated by Wenzel and Peters [19]. By using a G-equation model of the flame surface with added heat release, they were able to compute the two corresponding components of turbulent velocity fluctuations $u'' = u''_f + u''_g$. The shift in favour of the gas expansion induced fluctuations u''_g as opposed to the flow field fluctuations u''_f explained the CG/G transition recorded between two separate simulation cases. While in their work the gas expansion factor τ was varied, here the turbulence intensity u' is varied with τ held constant across the dataset. Hence, $u''_g = g(\tau s_L)$ and its corresponding flux component $\widetilde{u''_g c''}$ is expected to be constant, while $u''_f = f(u')$ and $\widetilde{u''_f c''}$ are expected to change as u' increases from case I to case V. The shift in balance between these quantities accompanies the CG/G transition recorded in the present dataset.

The CG/G transition observed in Fig. 6 is illuminated in the present work by decomposing the net scalar flux $\widetilde{u''c''}$ into the underlying velocity fluctuations u'' and the scalar fluctuations c''. The correlation between these two sets of fluctuations is shown for case I (with CG transport in Fig. 8a) and for case V (with G transport in Fig. 8b) respectively. For clarity, each point is coloured by the local progress variable value c (blue: leading edge, and red: trailing edge) as well as sized by the local reaction rate value $\dot{\omega}$ (small: low reaction rate,

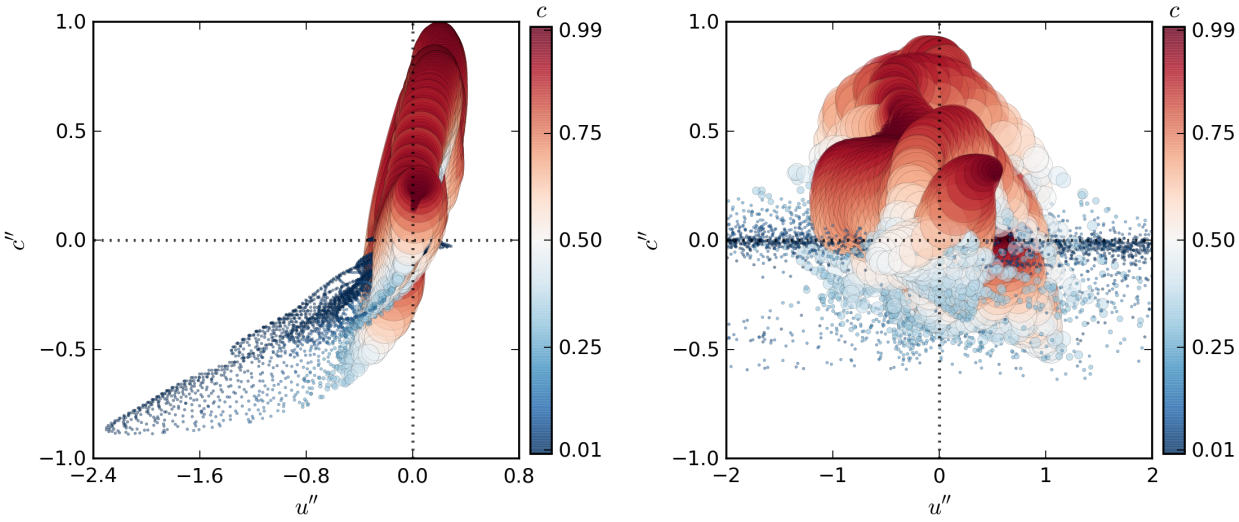

(a) u'' versus c'' at $u' = 1.5s_L$

(b) u'' versus c'' at $u' = 30s_L$

FIG. 8: A transition in the scalar flux transport mechanism (CG/G) evident in the changing correlation between u'' and c'' from case I (a) to V (b).

big: high reaction rate). This helps emphasise the changes local to the preheat zone and the reaction zone, i.e. within $0.6 < c < 0.9$ which is the region referred to in DH2 (as discussed in Sec. I B).

In case I (Fig. 8a, low u'), u'' and c'' are positively correlated through most of the flame brush. Either $u'' < 0$ and $c'' < 0$ (seen in the long trail of blue dots from the leading edge) or $u'' > 0$ and $c'' > 0$ (seen predominantly in the big red dots of the reaction zone region). A small number of points (in the preheat and reaction zones) display a negative correlation, but their contribution to the mean scalar flux $\widetilde{u''c''}$ is insignificant as the corresponding correlations do not carry over to the averaged values (shown in Fig. 6a). A more complicated correlation is evident in case V (Fig. 8b, high u') which exhibits G transport. Regions with positive correlations continue to be present, indicating the constant contribution of gas expansion in both cases. On the other hand, a large portion of the preheat and reaction zone shifts to a negative correlation, representing the overturning of this contribution by the turbulent flow field. In fact, the negative correlations are more significant in the mean (as seen in Fig. 6d). From the preceding discussion, it is clear that this qualitative change in the different behaviour of the scalar flux $\widetilde{u''c'}$ occurs at a certain threshold u' between $10s_L$ and $20s_L$ within the dataset.

As mentioned in Sec I B, Veynante et al. [39] provided a simple criterion to delineate

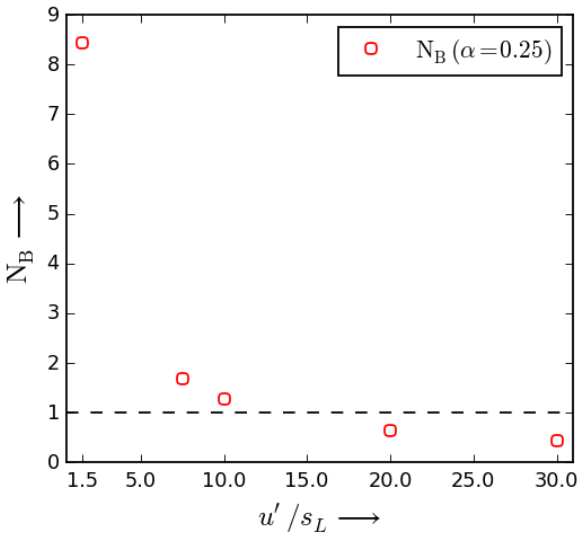

FIG. 9: The Bray number N_B for each case simulated in the present dataset delineating the gradient/contergradient regimes.

the CG/G regimes with contrasting $\widetilde{u''c'}$ behaviour. According to Eq. 9, $\widetilde{u''c'}$ has opposite signs across a Bray number of unity, $N_B \equiv \tau s_L/2\alpha u' = 1$. In the present context, u' is the only parameter relevant to the criterion that is being varied between any two cases. Moreover, the integral length scale ℓ_0 is also held constant ($\ell_0/\delta_L = 2.75$) across all the cases. The corresponding graph $N_B(u'/s_L)$ is shown in Fig. 9. With $\alpha = 0.25 \pm 0.1$, the predicted transition matches (to within $\pm 5 s_L$ between $10 s_L < u' < 20 s_L$) the transition observed between cases III (Fig. 6b)and IV (Fig. 6c). Veynante et al. [39] hypothesised α to be a function of ℓ_0/δ_L. Ignoring further the possible dependence on u'/s_L, they found that $N_B = 1$ delineates the CG/G transition in their dataset for $\alpha(\ell_0/\delta_L = 11) = 0.5$. The present analysis, with $\alpha(\ell_0/\delta_L \approx 3) = 0.25$, indicates that α (if it is monotonic) is a gradually increasing function of ℓ_0/δ_L. xA recent experimental investigation [55] of counter-gradient transport in V-shaped flames suggests a logarithmic variation of α with ℓ_0/δ_L supporting the assumption of a monotonic variation considered here. Kheirkhah and Gülder [55] further report $\alpha(\ell_0/\delta_L = 4) \approx 0.3$ which is very close to the values obtained here. This value of α, therefore, provides a valuable datapoint pertinent to subsequent investigations on the general behaviour of the efficiency function α. It is noted that the CG/G transition is reported here for a planar flame, and such transitions may occur locally and under slightly different conditions for more complicated geometries. For example, Kheirkhah and Gülder [55] observe a CG/G transition at $u'/s_L \approx 3$ which is lower than the conditions $u'/s_L \approx 10$

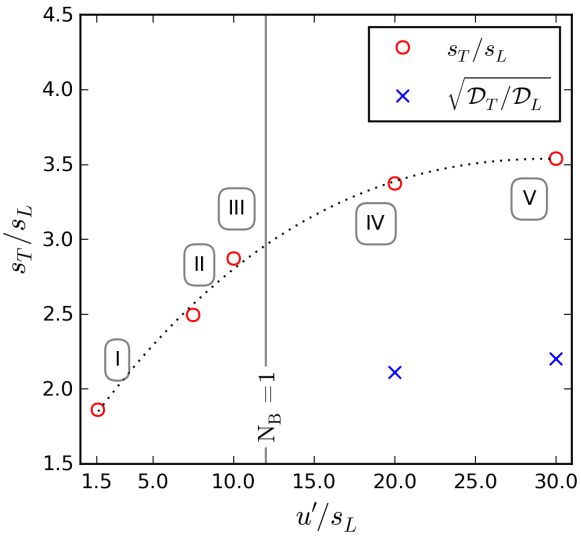

FIG. 10: Computed normalized turbulent burning velocity s_T/s_L compared with the value predicted by DH2 as allowed within the gradient diffusion regime.

observed here. This forms part of ongoing work focused on isolating configuration effects on flame propagation using DNS datasets of various geometries including V-shaped flames. The shift in balance between τ and u' in the CG/G transition at $\mathrm{N_B}(\alpha = 0.25) = 1$ occurs as u' is increased with ℓ_0 held constant in this dataset. Hence, the recorded CG/G transition is linked to a transition in the role of turbulence small-scales across $\mathrm{N_B} = 1$.

DH2 states that the role of "fine-body turbulence of size $\ell \ll \delta_L$" is to enhance s_T "by amplifying the microscopic (diffusive) transport processes" within the flame brush. As discussed above, $\widetilde{u''c''} < 0$ only in a small portion of the dataset corresponding to the cases IV and V (as shown in Fig. 9). Numerical evaluation of Eq. 8 for these cases is shown in Fig. 10. For the remaining cases, $\mathrm{N_B} > 1$ and the diffusion coefficient $\mathcal{D}_T < 0$. Hence, Eq. 8 cannot be evaluated. In other words, Damköhler's second hypothesis (DH2) applies strictly to the gradient transport regime where $\mathrm{N_B} < 1$.

Consequently, it appears that the general claim that "turbulence always acts to enhance the flame speed" might only apply in certain special limiting conditions. In fact, for $\mathrm{N_B} > 1$, the turbulence scales may have an inhibitive effect on s_T because $\widetilde{u''c''} > 0$ is transported against the gradient $-\partial\tilde{c}/\partial x$ favourable to flame propagation. The difference between values of $\sqrt{\mathcal{D}_T/\mathcal{D}_L}$ and s_T/s_L in Fig. 10 opens a further question: to what extent do DH1 and DH2 influence s_T individually in this region of overlapping validity? As yet, the evidence is inconclusive and further investigation is necessary to understand fully the significance

of DH1 and DH2 in the thin reaction zones regime. An investigation of higher u' will help understand when it is that the diffusive processes begin to govern decisively the enhancement in s_T. The present analysis elucidates, instead, the minimal criteria for the applicability of Damköhler's second hypothesis.

Brief Summary: CG/G Transition, DH1 and DH2

In low u' turbulence, DH1 applies and turbulent motion both roughens and stabilizes the surface. These simultaneous effects result in a positive correlation between u'' and c'', i.e. CG transport prevails. Referring to Eq. 7, this implies that the l.h.s. $\widetilde{u''c''} > 0$ whereas the r.h.s. $\partial\tilde{c}/\partial x > 0$. Hence, since $\mathcal{D}_T < 0$, it is clear that DH2 cannot operate.

In high u' turbulence, DH1 continues to apply as the large-scales serve to deform the surface. In this regime, however, G transport ($\widetilde{u''c''} < 0$) prevails. Hence, DH2 is applicable and operates alongside DH1. The transition between CG/G transport, therefore, delineates the regimes of applicability of DH2.

VI. CONCLUSION

Damköhler's first and second hypotheses (DH1 and DH2) are revisited in light of the bending effect of $s_T(u')$ recorded in a DNS dataset [24]. While DH1 remains valid before and after the bend [24], DH2 has limited validity within the dataset. The limitation emerges from a transition (from CG to G transport [39, 56]) in the behaviour of the turbulent scalar flux $\widetilde{u''c''}$ as turbulence intensity u' is varied across the dataset. The CG/G transition occurs for a Bray number $\mathrm{N_B} = 1$ at which u' balances gas expansion τ. In u' lower than this threshold value ($\mathrm{N_B} > 1$), the balance shifts in favour of CG transport. The resulting change in correlation between velocity u'' and scalar fluctuations c'' (which together constitute $\widetilde{u''c''}$) imposes a constraint on the validity of DH2.

Hence, contrary to Damköhler's original conclusion, it appears that "fine-body turbulence with $\ell \ll \delta_L$" may not always act to enhance the propagation speed s_T by "amplifying microscopic transport processes." In fact, this is plausible solely beyond the threshold u' (i.e. for $\mathrm{N_B} < 1$) in a regime where G transport prevails.

Two aspects solicit further investigation: 1) the nature (positive or negative) of effect

of "fine-body" turbulence $\ell \ll \delta_L$ on s_T below the threshold u' (i.e. for $\mathrm{N_B} > 1$) and its associated expression, and 2) the underlying causes that govern the shift between different effects of turbulence on flame propagation.

VII. ACKNOWLEDGEMENTS

The authors are grateful to UKCTRF and Archer for the computational support. GVN would like to thank the Cambridge Commonwealth European and International Trust and the Cambridge Philosophical Society for funding support.

[1] G.Damköhler. Der einfluss der turbulenz auf die flammengeschwindigkeit in gasgemschen. *Zeitschrift für Elektrochemie und angewandte physikalische Chemie*, 46:601–652, 1940.

[2] G.Damköhler. The effect of turbulence on the flame velocity in gas mixtures. Technical Report NACA-TM-1112, National Advisory Committee for Aeronautics, Washington DC, USA, 1947.

[3] B.Karlovitz, D.Denniston, D.Knapschaefer, and F.Wells. Studies on turbulent flames: A. flame propagation across velocity gradients b. turbulence measurement in flames. 4^{th} *Symposium (International) on Combustion*, 4(1):613–620, 1953.

[4] A.Klimov. Laminar flames in turbulent flow. *Zhournal Prikladnoi Mechaniki i Tekhnicheskoi Fiziki*, 3:49–58, 1963.

[5] C. K.Law. Dynamics of stretched flames. 22^{nd} *Symposium (International) on Combustion*, 22:1381–1402, 1989.

[6] K. N. C.Bray. Studies of the turbulent burning velocity. 431(1882):315–335, 1990.

[7] K. N. C.Bray and R. S.Cant. Some Applications of Kolmogorov's Turbulence Research in the Field of Combustion. *Proceedings of the Royal Society A: Mathematical, Physical and Engineering Sciences*, 434:217–240, 1991.

[8] S. B.Pope. The evolution of surfaces in turbulence. *International Journal of Engineering Science*, 26:445–469, 1988.

[9] S. M.Candel and T. J.Poinsot. Flame stretch and the balance equation for the flame area. *Combustion Science and Technology*, 70:1–15, 1990.

[10] U.Frisch. *Turbulence*. Cambridge University Press, 2004.

[11] D.Bradley, M.Lawes, and M. S.Mansour. The problems of the turbulent burning velocity. *Flow, Turbulence and Combustion*, 87(2-3):191–204, 2011.

[12] D.Bradley. How fast can we burn? 24^{th} *Symposium (International) on Combustion*, 24:247–262, 1992.

[13] A.Lipatnikov and J.Chomiak. Turbulent flame speed and thickness: phenomenology, evaluation, and application in multi-dimensional simulations. *Progress in Energy and Combustion Science*, 28:1–74, 2002.

[14] J. F.Driscoll. Turbulent premixed combustion: Flamelet structure and its effect on turbulent burning velocities. *Progress in Energy and Combustion Science*, 34:91–134, 2008.

[15] R.Abdel-Gayed, D.Bradley, M.Hamid, and M.Lawes. Lewis number effects on turbulent burning velocity. In *Symposium (International) on Combustion*, volume 20, pages 505–512. Elsevier, 1985.

[16] T.Poinsot, D.Veynante, and S.Candel. Diagrams of premixed turbulent combustion based on direct simulation. 23^{rd} *Symposium (International) on Combustion*, 23:613–619, 1991.

[17] J.Duclos, D.Veynante, and T.Poinsot. A comparison of flamelet models for premixed turbulent combustion. *Combustion and Flame*, 95:101–117, 1993.

[18] C.Meneveau and T.Poinsot. Stretching and quenching of flamelets in premixed turbulent combustion. *Combustion and Flame*, 86:311–332, 1991.

[19] H.Wenzel and N.Peters. Direct numerical simulation and modeling of kinematic restoration, dissipation and gas expansion effects of premixed flames in homogeneous turbulence. *Combustion Science and Technology*, 158:273–297, 2000.

[20] J. B.Bell, M. S.Day, J. F.Grcar, M. J.Lijewski, J. F.Driscoll, and S. A.Filatyev. Numerical simulation of a laboratory-scale turbulent slot flame. *Proceedings of the combustion institute*, 31(1):1299–1307, 2007.

[21] A. Y.Poludnenko and E.Oran. The interaction of high-speed turbulence with flames: Turbulent flame speed. *Combustion and Flame*, 158:301–326, 2011.

[22] H.Wang, E. R.Hawkes, and J. H.Chen. Turbulence-flame interactions in dns of a laboratory high karlovitz premixed turbulent jet flame. *Physics of Fluids*, 28(9):095107, 2016.

[23] S. A.Filatyev, J. F.Driscoll, C. D.Carter, and J. M.Donbar. Measured properties of turbulent premixed flames for model assessment, including burning velocities, stretch rates, and surface densities. *Combustion and Flame*, 141:1–21, 2005.

[24] G. V.Nivarti and R. S.Cant. Direct numerical simulation of the bending effect in turbulent premixed flames. *Proceedings of the Combustion Institute*, 36:1903–1910, 2017.

[25] H.Wang, E. R.Hawkes, B.Zhou, J. H.Chen, Z.Li, and M.Aldén. A comparison between direct numerical simulation and experiment of the turbulent burning velocity-related statistics in a turbulent methane-air premixed jet flame at high Karlovitz number. *Proceedings of the Combustion Institute*, 36:2045–2053, 2016.

[26] Ö. L.Gülder and G. J.Smallwood. Flame surface densities in premixed combustion at medium to high turbulence intensities. *Combustion Science and Technology*, 179:191–206, 2007.

[27] F. T.Yuen and O. L.Gülder. Turbulent premixed flame front dynamics and implications for limits of flamelet hypothesis. *Proceedings of the Combustion Institute*, 34:1393–1400, 2013.

[28] A. J.Aspden, M. S.Day, and J. B.Bell. Turbulence-flame interactions in lean premixed hydrogen: transition to the distributed burning regime. *Journal of Fluid Mechanics*, 680:287–320, 2011.

[29] B.Savard and G.Blanquart. Broken reaction zone and differential diffusion effects in high karlovitz n-c_7h_16 premixed turbulent flames. *Combustion and Flame*, 162(5):2020–2033, 2015.

[30] S.Lapointe, B.Savard, and G.Blanquart. Differential diffusion effects, distributed burning, and local extinctions in high karlovitz premixed flames. *Combustion and Flame*, 162(9):3341–3355, 2015.

[31] B.Lewis and G.Von Elbe. *Combustion, flames and explosions of gases*. Cambridge University Press, 1938.

[32] F.Williams. Progress in knowledge of flamelet structure and extinction. *Progress in Energy and Combustion Science*, 26(4):657–682, 2000.

[33] D.Veynante and L.Vervisch. Turbulent combustion modeling. *Progress in Energy and Combustion Science*, 28:193–266, 2002.

[34] K. N. C.Bray. *Turbulent flows with premixed reactants*, pages 115–183. Springer Berlin Heidelberg, 1980.

[35] S. B.Pope. *Turbulent flows*. IOP Publishing, 2001.

[36] P. A.Libby and K. N. C.Bray. Countergradient diffusion in premixed turbulent flames. *AIAA journal*, 19(2):205–213, 1981.

[37] C. J.Rutland and R. S.Cant. Turbulent transport in premixed flame. In *Proceedings of the Summer Program at the Centre for Turbulence Research, Stanford*. NASA Ames/Stanford

University, 1994.

[38] I. G.Shepherd, J. B.Moss, and K. N. C.Bray. Turbulent transport in a confined premixed flame. 19(1):423–431, 1982.

[39] D.Veynante, A.Trouvé, K. N. C.Bray, and T.Mantel. Gradient and counter-gradient scalar transport in turbulent premixed flames. *Journal of Fluid Mechanics*, 332:263–293, 1997.

[40] D. S.Louch and K. N. C.Bray. Vorticity in unsteady premixed flames: vortex pair-premixed flame interactions under imposed body forces and various degrees of heat release and laminar flame thickness. *Combustion and flame*, 125:1279–1309, 2001.

[41] T. M.Wabel, A. W.Skiba, and J. F.Driscoll. Turbulent burning velocity measurements: Extended to extreme levels of turbulence. *Proceedings of the Combustion Institute*, 36:1801–1808, 2016.

[42] R. S.Rogallo. Numerical experiments in homogeneous turbulence. Technical Report NASA TM 81315, NASA Ames Research Center, CA, 1981.

[43] G. K.Batchelor and A. A.Townsend. Decay of Turbulence in the Final Period. *Proceedings of the Royal Society A: Mathematical, Physical and Engineering Sciences*, 194:527–543, 1948.

[44] T.Poinsot, S.Candel, and A.Trouvé. Applications of direct numerical simulation to premixed turbulent combustion. *Progress in Energy and Combustion Science*, 21(6):531–576, 1995.

[45] N.Swaminathan and R. W.Grout. Interaction of turbulence and scalar fields in premixed flames. *Physics of Fluids*, 18(4):045102, 2006.

[46] U.Ahmed, R.Prosser, and A. J.Revell. Towards the development of an evolution equation for flame turbulence interaction in premixed turbulent combustion. *Flow, turbulence and combustion*, 93(4):637–663, 2014.

[47] M. D.Smoke and V.Giovangigli. Formulation of the premixed and nonpremixed test problems. In *Reduced Kinetic Mechanisms and Asymptotic Approximations for Methane-Air Flames*, pages 1–28. Springer, 1991.

[48] A.Aspden, M.Day, and J.Bell. Turbulence-chemistry interaction in lean premixed hydrogen combustion. *Proceedings of the Combustion Institute*, 35(2):1321–1329, 2015.

[49] R. S.Cant. SENGA2: User guide. Technical Report CUED-THERMO-2012/04 - 2, Cambridge University Engineering Department, 2013.

[50] J. C.Sutherland and C. A.Kennedy. Improved boundary conditions for viscous, reacting, compressible flows. *Journal of Computational Physics*, 191:502–524, 2003.

[51] C. A.Kennedy and M. H.Carpenter. Additive Runge-Kutta schemes for convection-diffusion-reaction equations. *Applied Numerical Mathematics*, 44:139–181, 2003.

[52] L.Prandtl. Bericht über untersuchungen zur ausgebildeten turbulenz. *Z. angew. Math. Mech.*, 5:136–139, 1925.

[53] S.Lapointe and G.Blanquart. Fuel and chemistry effects in high karlovitz premixed turbulent flames. *Combustion and Flame*, 167:294–307, 2016.

[54] N.Chakraborty and R. S.Cant. Effects of lewis number on scalar transport in turbulent premixed flames. *Physics of Fluids*, 21(3):035110, 2009.

[55] S.Kheirkhah and Ö. L.Gülder. Consumption speed and burning velocity in counter-gradient and gradient diffusion regimes of turbulent premixed combustion. *Combustion and Flame*, 162(4):1422–1439, 2015.

[56] K. N. C.Bray. Turbulent transport in flames. In *Proceedings of the Royal Society of London A: Mathematical, Physical and Engineering Sciences*, volume 451, pages 231–256, 1995.